Supporting Information for

Sequential Multiscale Simulation of Filtering Facepiece for Prediction of Filtration Efficiency and Resistance in Varied Particulate Scenarios

Kyeongeun Lee,[†,‡] Yeon-Woo Jung,[‡] Hanjou Park,[†] Dongmi Kim[§] and Jooyoun Kim[,†,∥]*

[†]Department of Textiles, Merchandising and Fashion Design, Seoul National University, Seoul 08826, Korea

[‡]Reliability Assessment Center, FITI Testing & Research Institute, Seoul 07791, Korea

[§]Digital Material Laboratory, Trinity Engineering, Seoul 07997, Korea

[∥] Research Institute of Human Ecology, Seoul National University, Seoul 08826, Korea

* E-mail: jkim256@snu.ac.kr.

9 pages, 5 sections, 7 figures

Section 1: Filtration Test

The filtration test parameters for filter media and facepiece are shown in Figure S1.

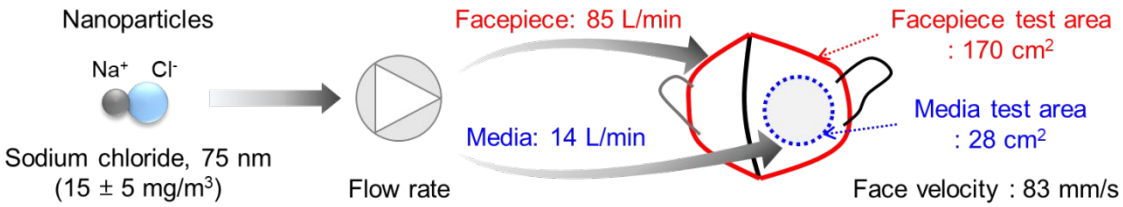

Figure S1. Filtration test parameters for filter media and filtering facepiece.

Section 2: Reconstruction of Filter Media

X-ray computed tomography (Xμ-CT) was performed on the filter media layers using Zeiss X-Radia 510 Versa (Zeiss, Germany).[1] Figure S2 demonstrates the workflow of 3D reconstruction from Xμ-CT images. For the entire layer construction, a voxel size of 2.0 μm was applied with the corresponding field of view of 2000 μm. For each layer of web, a voxel size of 0.8 μm was applied with the field of view of 800 μm. Approximately 1000 slices of 2D images were taken for 3D reconstruction. Image characterization was processed with Dragonfly Pro software (Object Research Systems, Canada). The filtering facepiece used in this study was comprised of one layer of meltblown filter web sandwiched between the spunbond webs (cover web and inner web). The mean diameters of fibers constituting the cover web, meltblown web, and inner web were 15.7 μm, 5.5 μm, and 18.7 μm, respectively.

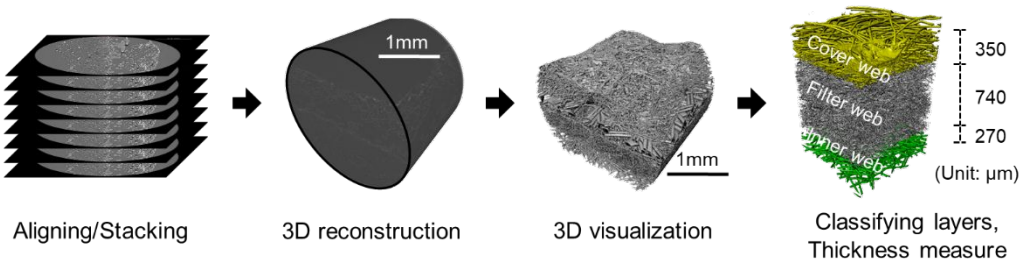

Figure S2. Workflow of reconstructions for 3D image.

Each layer of Xμ-CT image was imported using ImportGeo-Vol® module (Figure S3c and d). The imported image was permuted and rotated for alignment, so that the filter layer's cross-section and the web surface were placed in x-z plane and in x-y plane, respectively. Each layer was cropped into 625 × 625 voxels in the x-y plane, and the z axis domains were cut out corresponding to the thickness (Figure S3e). The segmentation was performed by using a single threshold filter to separate the solid (fiber) region from the non-solid region (Figure S3f). Three layers of reconstructed models were combined in a 3-layer media construction (500 μm × 500 μm × 1350 μm) using LayerGeo® module (Figure S3g and h). In the constructed model, a regular hexahedral voxel was used, and the grid length was configured to be 5 to 26 times smaller than the fiber diameter so that a fiber had at least 5 layers of grids (Figure S4).

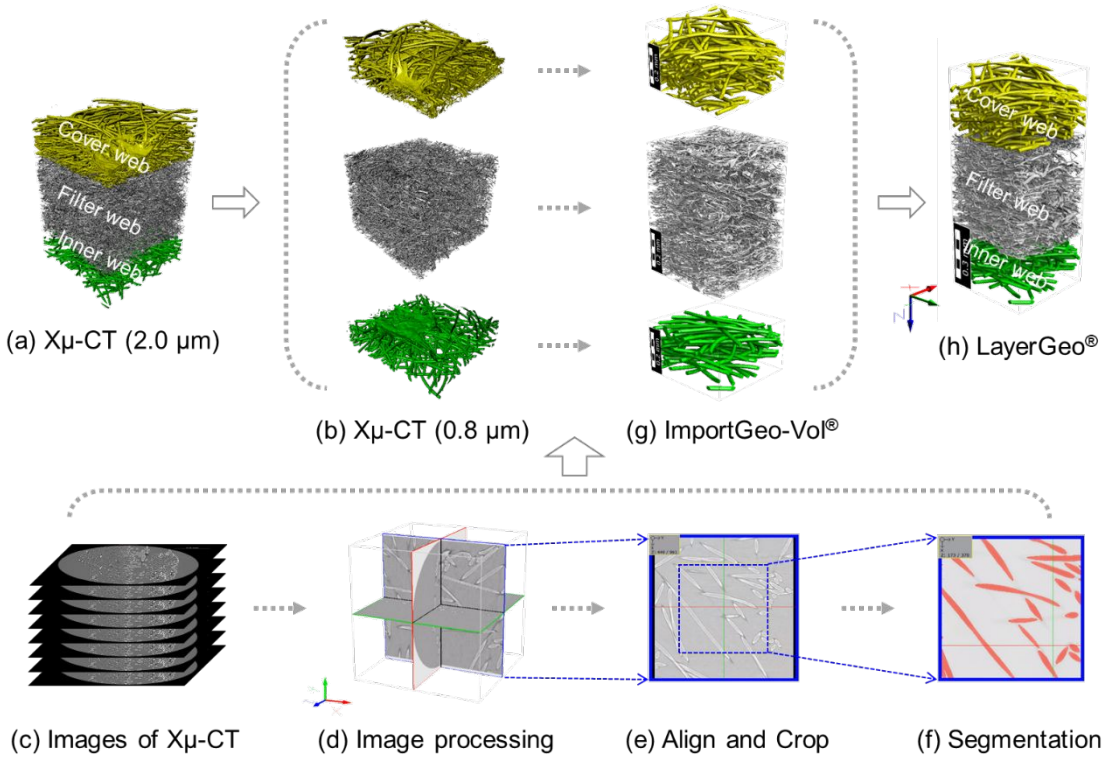

Figure S3. Steps for importing the facepeice layers into GeoDict®, based on Xμ-CT images. (a) Entire layer analyzed by Xμ-CT with a voxel size of 2.0 μm. (b) Each layer with a voxel size of 0.8 μm. (c) Original slice images from the Xμ-CT. (d) Imaging processing. (e) Align and crop. (f) Segment images using the single threshold filter (fibers are shown in red). (g) Reconstruction of layers to form a 3D model. (h) The entire layers stacked; final structure for flow simulation.

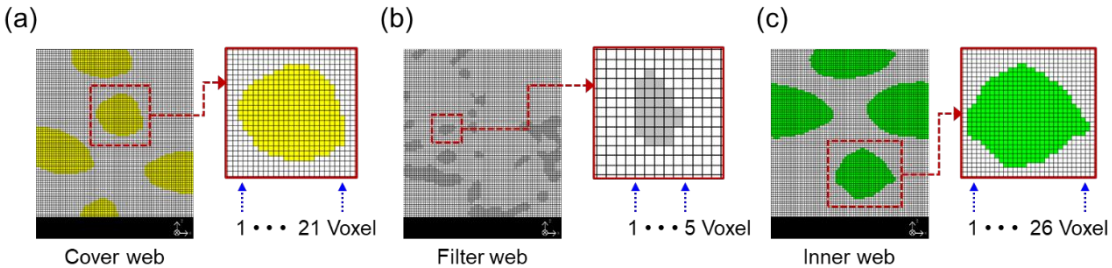

Figure S4. Grid length of constructed webs. (a) Cover web. (b) Filter web. (c) Inner web.

Section 3: Reconstruction of Filtering Facepiece

Figure S5 indicates the procedure of 3D reconstruction of a filtering facepiece. A filtering facepiece loaded on a test jig was reverse engineered by 3D scanning, using an optical non-contact scanner (Go!SCAN 50, Creaform Inc., Canada).[2] The scanned mesh data of 0.5 mm resolution was generated in real-time via VXelement software connected with the 3D scanner. The virtual facepiece model was created with 139,755 triangular elements, and the derived model was imported into GeoDict® using the ImportGeo-CAD® module. Since the scanned model was filled with solid inside the filtering facepiece, 'Erode,' 'Dilate,' and 'Reassign' functions in the ProcessGeo® module were used to remove the materials inside the facepiece and to leave only the materials in layers' thickness. The rectangular test jig was generated reflecting the actual test procedure by utilizing 'Flood-Fill Component Plane' and 'Edit in Paint' functions. After the filtering facepiece model and the test jig model were merged, the combined 3D model was employed in later simulations for filtration performance.

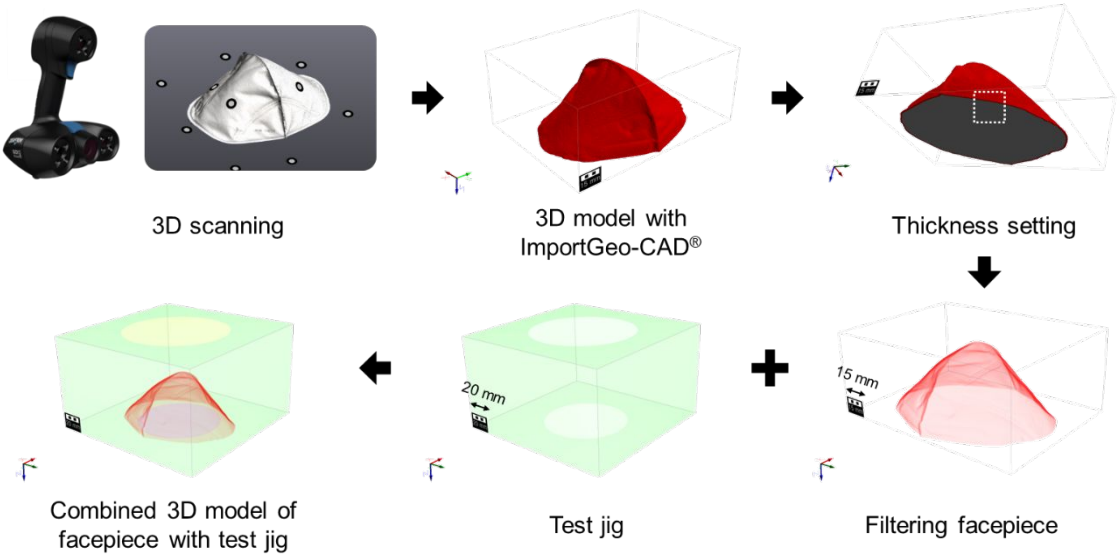

Figure S5. Procedure of reconstruction of filtering facepiece with a test jig.

Figure S6a shows the computational domain with dimensions and boundary conditions. A boundary condition of L × W × H = 17 × 17 × 10 cm^3 was created, and the velocity inlet and pressure outlet were set in consideration of the flow direction. The diameters of the inlet and outlet circles of 11 cm and 9 cm, respectively, were generated mimicking the jig holes. The optimal number of voxels was calculated by performing the voxel resolution test, and the simulation was performed based on the result. A comprehensive representation of a computational voxel for filtering facepiece with test jig was displayed in Figure S6b. Considering the accuracy and computational cost, a voxel length of 0.5 mm was chosen, where three or more voxels could construct a thickness of filtering facepiece. The total number of voxels consisting of the facepiece and the jig was 2.7×10^7.

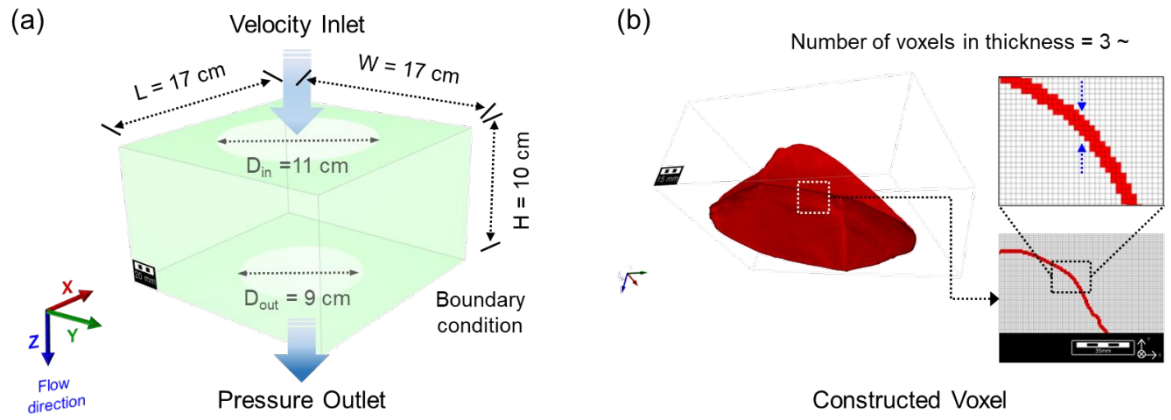

Figure S6. Computational domain and dimension. (a) Boundary conditions of a filtering facepiece with test jig. (b) Voxel parameters for the thickness of a filtering facepiece.

Section 4: Filtration Simulation

The transport of the particles during the filtration simulation was obtained by applying the Lagrangian Particle Tracking method.[3] It was assumed that the dispersed two-phase flow is diluted and the flowing particles have no effect on the flow. That is, the distance between particles in the air was large enough to ignore the particle-particle collisions. NaCl particles were simplified in a spherical shape, and each particle was assumed to move by the Stokes drag force and the Brownian motion. The movement of particles was obtained by solving eq S1 and S2, where m is particle mass (kg), $\vec{v}$ is particle velocity (m/s), t is time (s), μ_a is air dynamic viscosity (kg/m·s), R is particle radius (m), $\vec{u}$ is fluid velocity (m/s), D is diffusivity (m²/s), $d\vec{W}$ is 3D Wiener measure ($\sqrt{s}$), C_c is the Cunningham correction factor, λ is mean free path.[4] The particle's initial position was set to be in the inflow region, and the size distribution was in the range of 50 nm ~ 18 μm referring to the environmental conditions.

$$m\frac{d\vec{v}}{dt} = 6\pi\mu_a\frac{R}{C_c}\left(\vec{u} - \vec{v} + \sqrt{2D}\frac{d\vec{W}(t)}{dt}\right) \qquad \text{(S1)}$$

$$C_c = 1 + \frac{\lambda}{R}\left(1.17 + 0.525e^{-0.78\frac{R}{\lambda}}\right) \qquad \text{(S2)}$$

Section 5: Quality Factor of Filter Media

Quality factor (QF) of filter media was calculated to evaluate the relative filtration efficiency at a unit resistance, following eq. S3.

$$Quality\ factor\ (Pa^{-1}) = \frac{-\ln\ (\%\ penetration\ /\ 100\%)}{pressrue\ drop\ (Pa)} \qquad \text{(S3)}$$

Applying the simulated test results of penetration and resistance shown in Figure 7, QF was calculated as a function of accumulated challenged mass, for the varied environmental conditions (Figure S7). The result of NIOSH condition showed the lowest QF, in which resistance increased rapidly and penetration was relatively high. The QF of work area was highest because of lower resistance and lower penetration than other conditions. QF of filter web depended on the particle size distribution and mass concentration.

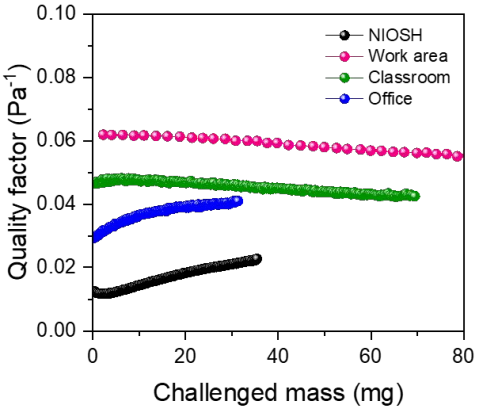

Figure S7. Quality factor of filter web based on the simulated test results.

REFERENCES

1. Jung, S.; Hemmatian, T.; Song, E.; Lee, K.; Seo, D.; Yi, J.; Kim, J., Disinfection Treatments of Disposable Respirators Influencing the Bactericidal/Bacteria Removal Efficiency, Filtration Performance, and Structural Integrity. *Polymers (Basel)* **2020,** *13* (1), 45.
2. Affatato, S.; Ruggiero, A.; De Mattia, J. S.; Taddei, P., Does metal transfer affect the tribological behaviour of femoral heads? Roughness and phase transformation analyses on retrieved zirconia and BioloxB® Delta composites. *Composites. Part B, Engineering* **2016,** *92*, 290-298.
3. Guha, A., Transport and Deposition of Particles in Turbulent and Laminar Flow. *Annual Review of Fluid Mechanics* **2008,** *40* (1), 311-341.
4. Math2market, FilterDict Handbook, GeoDict 2021 from Math2Market GmbH, Germany. **2021**, https://doi.org/10.30423/userguide.geodict2021-FilterDict.